Title
Image guided laser ablation of demineralization from root surfaces

Authors
Dhillon, Navitinder
Chan, Kenneth H
Yang, Vincent B
et al.

Publication Date
2019-02-01

DOI
10.1117/12.2512938

Peer reviewed

HHS Public Access

Author manuscript

Proc SPIE Int Soc Opt Eng. Author manuscript; available in PMC 2019 April 17.

Published in final edited form as:

Proc SPIE Int Soc Opt Eng. 2019 February ; 10857: . doi:10.1117/12.2512938.

Image guided laser ablation of demineralization from root surfaces

Navitinder Dhillon, **Kenneth H. Chan**, **Vincent B. Yang**, and **Daniel Fried**

University of California, San Francisco, San Francisco, CA 94143-0758

Abstract

It is challenging to identify demineralized areas of root lesions due to cervical erosion, calculus formation, and heavy staining of dentin. We have found that root caries can be imaged with extremely high contrast at short wavelength IR (SWIR) wavelengths beyond 1500-nm. Lasers are well suited for the selective removal of caries lesions from tooth surfaces. A CO_2 laser operating at a wavelength of 9.3-μm was combined with a thulium-doped fiber laser operating at 1880-nm for the selective removal of root caries lesions from extracted teeth. Serial SWIR reflectance images at 1880-nm were used to guide the CO_2 laser for image-guided laser ablation. Cross polarization optical coherence tomography (CP-OCT) was used to assess the initial depth of the lesions before removal and assess the volume of sound and demineralized tissue removed by the CO_2 laser. With this image-guided approach, we believe we can achieve highly selective lesion removal and minimal damage to surrounding sound tissues.

Keywords

root caries; SWIR reflectance imaging; image-guided laser ablation

1. INTRODUCTION

Multiple studies both *in vitro* and *in vivo* on the coronal surfaces of teeth have demonstrated that short wavelength infrared (SWIR) reflectance imaging yields higher contrast between demineralized and sound tooth structure than visible reflectance and fluorescence. Much of this difference is due to the lack of interference from stains at wavelengths longer than 1200-nm [1–6]. SWIR wavelengths appear to be equally advantageous for imaging root caries and calculus due to the lack of interference of stains beyond 1200-nm and increased suppression of the reflectivity from the sound dentin due to higher water absorption which increases markedly beyond 1400-nm [7]. Therefore, SWIR reflectance images of root surfaces can potentially be used to guide lasers for the selective removal of demineralization for the treatment of root caries.

Lasers are well designed for the selective removal of caries lesions. They can be used to precisely remove thin layers of demineralized enamel if a small spot size is used. Studies have demonstrated that CO_2 lasers (λ = 9.3– 9.6-μm) are ideal for caries removal and have added benefits, namely, the thermal modification of dental hard tissues for higher resistance to further decay [8]. Typical dental lasers are operated by hand, which nullifies their capacity for high precision and selectivity. Thus, an image-guided computer-controlled laser is ideal

for selectively removing caries lesions. Previous work demonstrated that the CO_2 laser irradiated enamel does not interfere with the ability to image the tooth surface nor significantly distort the contrast between sound and carious dental hard tissues [9]. Furthermore, in past SWIR image-guided laser experiments, InGaAs cameras were successful in detecting lesion presence and guiding a CO_2 laser for lesion removal [10]. However this technique had limitations, it was challenging to precisely align SWIR reflectance images with the laser and InGaAs cameras are currently expensive. Last year we demonstrated that the CO_2 laser beam can be combined with a SWIR thulium fiber laser to improve lesion detection and ablation alignment [11, 12]. A less expensive extended range InGaAs photodiode was used to capture backscattered light at wavelengths beyond 1700-nm. This method also is advantageous for improving the signal throughput for improved lesion detection. The purpose of this study is to demonstrate that we can use this system to selectively remove demineralization from root surfaces in addition to tooth coronal surfaces.

2. MATERIALS AND METHODS

2.1 Sample and Lesion Preparation

Eight human teeth with suspected root caries were collected and sterilized with gamma radiation. Samples were stored in a moist environment of 0.1% thymol to maintain tissue hydration and prevent bacterial growth. Color and SWIR images of one of the tooth samples is shown in Fig. 1.

2.2 Integrated CO_2 Laser and SWIR Point-to-Point Imaging System

A diagram of the system is shown in Fig. 2. An RF-excited laser, DL-500 prototype from Access Laser Co (Everett, WA) operating at a wavelength of 9.3-μm was used with a pulse duration of 25-μs and a pulse repetition rate of 200-Hz. The laser energy output was monitored using a power/energy meter, ED-200 from Gentec (Quebec, Canada). The laser beam was focused to a beam diameter of 250-μm using a ZnSe lens of 100-mm focal length. A razor blade was scanned across the beam to determine the diameter ($1/e^2$) of the laser beam. The incident fluence was 31 J/cm^2. Computer-controlled XY galvanometers 6200HM series with MicroMax series 671 from Cambridge Technology, Inc. (Cambridge, MA) were used to create controlled movements of the samples during SWIR reflectance image acquisition and subsequent laser irradiation. A pressure air-actuated fluid spray delivery system consisting of a 780S spray valve, a Valvemate 7040 controller, and a water reservoir from EFD, Inc. (East Providence, RI) was used to provide a continuous and uniform spray of fine water mist (5 ml/mm) onto the tooth surfaces.

Point-to-point SWIR reflectance images were acquired before each CO_2 laser ablation scan by scanning at 1880-nm using a tunable 1850–1880-nm thulium fiber laser, Model TLT-5 from IPG photonics (Oxford, MA) with an output of 500-mW. The beam from the thulium fiber laser was combined with the CO_2 laser beam with a beamsplitter and focused with the same 100-mm focal length ZnSe lens onto the occlusal tooth surface.

A SWIR InGaAs photodiode detector, Model PDA10DT from Thorlabs (Newton, NJ) was used to collect backscattered SWIR light from the occlusal surface. Polarizers were placed

before the laser sources and the detector to remove specular reflection from the tooth surfaces.

2.3 Digital Microscopy

Tooth surfaces were examined after laser irradiation using an digital optical microscope - VHX-1000 from Keyence (Elmwood, NJ) with a VH-Z25 magnification lens. Depth composition digital microscopy images (DCDM) were acquired by scanning the image plane of the microscope and reconstructing a depth composition image with all points at optimum focus for displaying a fully focused 2D image. Images of the samples were acquired before and after ablation at 50x magnification.

2.4 OCT System

The cross-polarization OCT (CP-OCT) system used for this study was purchased from Santec (Komaki, Aichi, Japan). This system acquires only the cross polarization image, not both the cross and co-polarization images (PS-OCT). The Model IVS-3000-CP utilizes a swept laser source; Santec Model HSL-200–30 operating with a 30 kHz a-scan sweep rate. The Mac-Zehnder interferometer is integrated into the handpiece which also contains the microelectromechancial (MEMS) scanning mirror and the imaging optics. It is capable of acquiring complete tomographic images of a volume of 6 × 6 × 7 mm in approximately three seconds. The body of the handpiece is 7 × 18 cm with an imaging tip that is 4 cm long and 1.5 cm across. This system operates at a wavelength of 1321-nm with a bandwidth of 111-nm with a measured resolution in air of 11.4 μm (3 dB). The lateral resolution is 80-μm ($1/e^2$) with a transverse imaging window of 6 mm x 6 mm and a measured imaging depth of 7-mm in air. The polarization extinction ratio was measured to be 32 dB.

Acquired scans are compiled into *b-scan* files. Image processing was carried out using Igor Pro™, data analysis software from Wavemetrics Inc, (Lake Oswego, Oregon). The processed images were then analyzed using Avizo software (ThermoFisher, Hillsboro, OR).

2.5 Imaging, Processing, and Caries Removal

The algorithm used for image-guided removal is shown in Fig. 3. Each step of the algorithm is discussed below.

Samples were air-dried for ~10 seconds prior to SWIR point-to-point reflectance image acquisition of the tooth root surface. Images were acquired over an area 13×12-mm with a 50-μm pixel pitch. The backscattered SWIR intensity at each point was averaged over 5 acquisitions. Each point was rasterized into an 8-bit SWIR image. Highly scattering demineralized surfaces confer higher signal or appear brighter in the SWIR reflectance images, while sound tissues appear dark.

Lesion presence was automatically determined through analysis of the pixel intensity. Pixel intensities were analyzed through an Otsu's adaptive thresholding method (6 cluster groups). This automatically determines an intensity threshold by calculating the median intensity of each cluster and correlating the distance of each point's intensity to its respective clustering group. This method then groups pixels of similar intensity together.

As the lesion is removed, clustering becomes overly sensitive, therefore the initial SWIR image was appended to the newly acquired scanned images during lesion removal. The lesion pixels in the new image that are grouped with the lesion pixels in the initial image were subjected to laser treatment. A highly scattering reference target was scanned along with the sample as a reference of maximum signal from scattering so that sequential SWIR reflectance images can be normalized and compared with each other. Healthy sound enamel structure outside the artificially generated lesion was imaged to provide a positive control of sound tissue pixel intensity. A look-up-table (LUT) was created which maps out lesion areas demarcated for laser treatment. Using the acquired LUT, the CO_2 laser was scanned over the identified lesion area for removal. The distance between laser pulses was 50-μm, roughly 1/5 of the 250-μm laser spot diameter. Repeated serial SWIR images and LUTs were taken until the lesion was no longer discriminated. All image analysis was carried out using Labview from National Instruments (Austin, TX).

2.6 Selective Lesion Removal Analysis

Teeth were imaged before and after image-guided ablation with CP-OCT and digital microscopy. DCDM images were visually assessed for lesions before ablation and their removal after ablation. Initial and post-ablation CP-OCT scans, were assessed for lesion volume. The automated 3D lesion detection method is based on previous work and uses an automated edge detection routine to extract lesion volume [14, 15]. Additionally, CP-OCT scans were used to quantify laser ablation volume. Background subtraction was carried out by subtracting the mean with 5 standard deviations of the background that was selected from the top 10 pixels of 220 b-scans. These data points provided consistent background signal intensity and manifested a standard deviation less than 0.04 dB. A 50×50×2.56 anisotropic diffusion Gaussian smoothing filter was applied. In addition, a 3×3×3 rotating kernel transformation (RKT) technique was applied to emphasize lines and eliminate speckle noise. Surfaces were extracted by using a full width half maximum edge detection approach. Initial and post-ablation surfaces were 3D registered using an Iterative Closest Point algorithm. A linear interpolator was applied to the post-ablative (moving image) scans to fit the registered scans over the initial (fixed image) scans. Subtraction of the registered post-ablative scans from the initial surface scans was used to quantify ablation volume and process 2D ablation maps. These 2D ablation depth maps were compared to initial 2D lesion depth maps to assess selectivity. Furthermore, post-ablative 2D lesion depth maps were analyzed to determine complete lesion removal.

3. RESULTS AND DISCUSSION

Images from one of the samples before and after removal of the root lesion are shown in Fig. 4. This sample has a thin composite restoration and there is demineralization around the cervical margin of the restoration. The color images show stained areas around the composite and it is difficult to identify where the demineralization is located. Demineralization is clearly visible in the SWIR image with a large patch of demineralization located 1–2 mm from the base of the composite with a smaller area close to the composite. The OCT scan taken prior to laser ablation shows the depth of demineralization in those two areas. The SWIR image taken after removal shows that most of the large patch of

demineralization was removed while it is difficult to identify any differences before and after removal in the color images. The OCT image acquired after removal shows the depth of removal which matches the depth and position of the lesion before removal. OCT scans acquired before and after the removal of root caries lesions from eight tooth samples indicated that SWIR image guided laser ablation was successful in the removal of most of the demineralization from the root surfaces. This small pilot study indicates that image guided laser ablation is a promising approach for the selective removal of demineralization from root surfaces.

4. ACKNOWLEDGMENTS

We acknowledge Access Laser Co. for loan of the 9.3-μm CO_2 laser and Nathaniel Fried for loan of the thulium fiber laser. This work was supported by NIH/NIDCR Grant R01 -DE19631.

5. REFERENCES

[1]. Jones RS, Huynh GD, Jones GC, and Fried D, “Near-IR Transillumination at 1310-nm for the Imaging of Early Dental Caries,” Optics Express, 11(18), 2259–2265 (2003). [PubMed: 19466117]

[2]. Buhler C, Ngaotheppitak P, and Fried D, “Imaging of occlusal dental caries (decay) with near-IR light at 1310-nm,” Opt Express, 13(2), 573–82 (2005). [PubMed: 19488387]

[3]. Staninec M, Lee C, Darling CL, and Fried D, “In vivo near-IR imaging of approximal dental decay at 1,310 nm,” Lasers Surg Med, 42(4), 292–8 (2010). [PubMed: 20432277]

[4]. Chung S, Fried D, Staninec M, and Darling CL, “Multispectral near-IR reflectance and transillumination imaging of teeth “ Biomed Opt Express, 2(10), 2804–2814 (2011). [PubMed: 22025986]

[5]. Fried WA, Chan KH, Fried D, and Darling CL, “High Contrast Reflectance Imaging of Simulated Lesions onTooth Occlusal Surfaces at Near-IR Wavelengths,” Lasers Surg Med, 45(8), 533–541 (2013). [PubMed: 23857066]

[6]. Simon JC, Lucas SA, Lee RC, Staninec M, Tom H, Chan KH, Darling CL, and Fried D, “Near-IR Transillumination and Reflectance Imaging at 1300-nm and 1500–1700-nm for in vivo Caries Detection,” Lasers Surg Med, 48(6), 828–836 (2016). [PubMed: 27389018]

[7]. Yang VB, Curtis DA, Fried D, and “Cross-polarization reflectance imaging of root caries and dental calculus at wavelengths from 400–2350-nm,” J Biophotonics, 11, e201800113 (2018).

[8]. Konishi N, Fried D, Featherstone JDB, and Staninec M, “Inhibition of secondary caries by CO2 laser treatment,” Amer J Dent, 12(5), 213–216 (1999). [PubMed: 10649910]

[9]. LaMantia NR, Tom H, Chan KH, Simon JC, Darling CL, and Fried D, “High contrast optical imaging methods for image guided laser ablation of dental caries lesions,” Lasers in Dentistry XX Proc. of SPIE Vol. 8929(P) 1–7 (2014).

[10]. Chan KH, and Fried D, “Selective Removal of Demineralization Using Near Infrared Cross Polarization Reflectance and a Carbon Dioxide Laser,” Lasers in Dentistry XVIII. Proc Spie. Vol. 8208(U)1–8 (2012).

[11]. Chan KH, Fried NM, and Fried D, “Selective ablation of carious lesions using an integrated near-IR imaging system and a novel 9.3-μm CO2 Laser “ Lasers in Dentistry XXIV. Vol. Proc. SPIE Vol. 10473 (E)1–7 (2018).

[12]. Chan KH, and Fried D, “Selective ablation of dental caries using coaxial CO2 (9.3-μm) and near-IR (1880-nm) lasers,” Lasers Surg Med, doi: 10.1002/lsm.23002. [Epub ahead of print] (2019).

[13]. Bush J, Feldchtein F, Gelikonov G, Gelikonov V, and Piyevsky S, “Cost effective all-fiber autocorrelator for optical coherence tomography imaging,” 17th International Conference on Optical Fibre Sensors SPIE, Vol. 5855(1) 254–7 (2005).

[14]. Kang H, Jiao JJ, Chulsung L, Le MH, Darling CL, and Fried DL, "Nondestructive Assessment of Early Tooth Demineralization Using Cross-Polarization Optical Coherence Tomography," Selected Topics in Quantum Electronics, IEEE Journal of, 16(4), 870–876 (2010).

[15]. Lee RC, Kang H, Darling CL, and Fried D, "Automated assessment of the remineralization of artificial enamel lesions with polarization-sensitive optical coherence tomography," Biomed Opt Express, 5(9), 2950–62 (2014). [PubMed: 25401009]

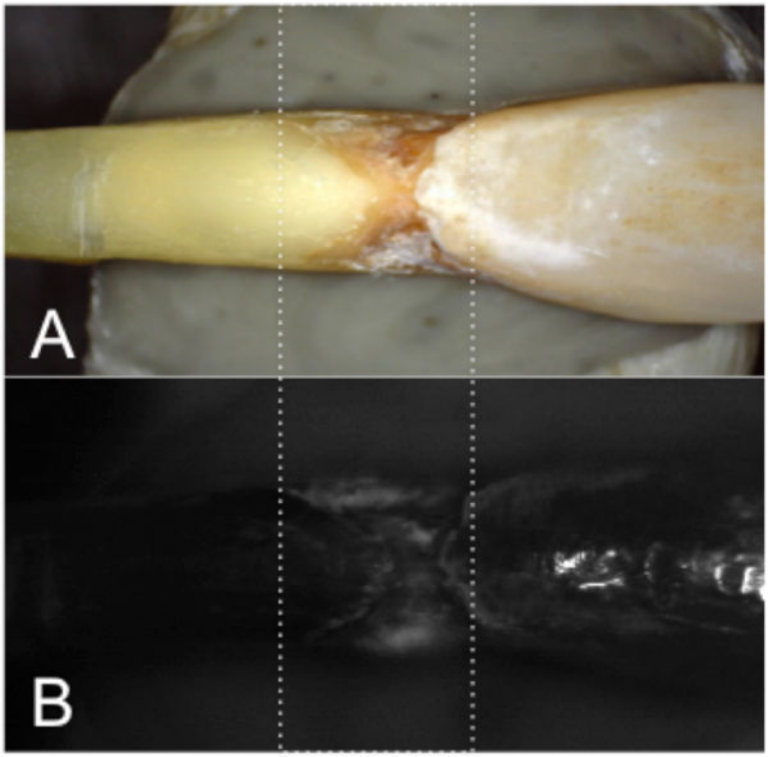

Fig. 1.
(A) Color and SWIR (1500–1750-nm) images of a tooth with root caries. The root caries lesion is located between the white dotted lines.

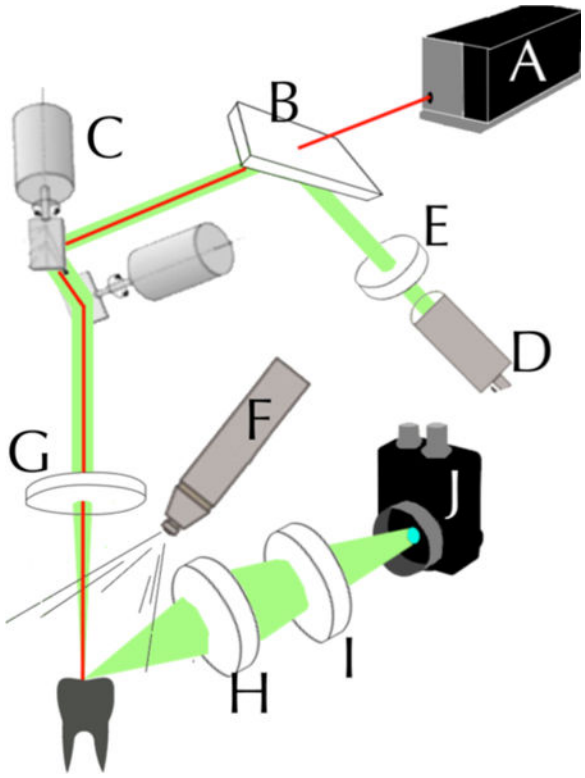

Fig. 2.

Combined SWIR image-guided caries ablation system: (A) CO_2 laser; (B) beamsplitter; (C) galvanometer mirror scanner; (D) near-IR fiber laser (1880-nm) w/ IR lens; (E) collimator; (F) water-/airspray; (G) scanning lens; (H) IR lens; (I) cross-polarizer; (J) SWIR photodetector; (Red line) CO_2 laser; (Green line) SWIR light.

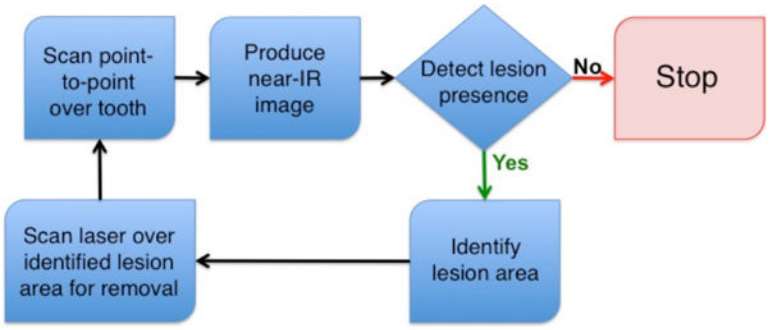

Fig. 3.
Flow-chart of image-guided ablation protocol.

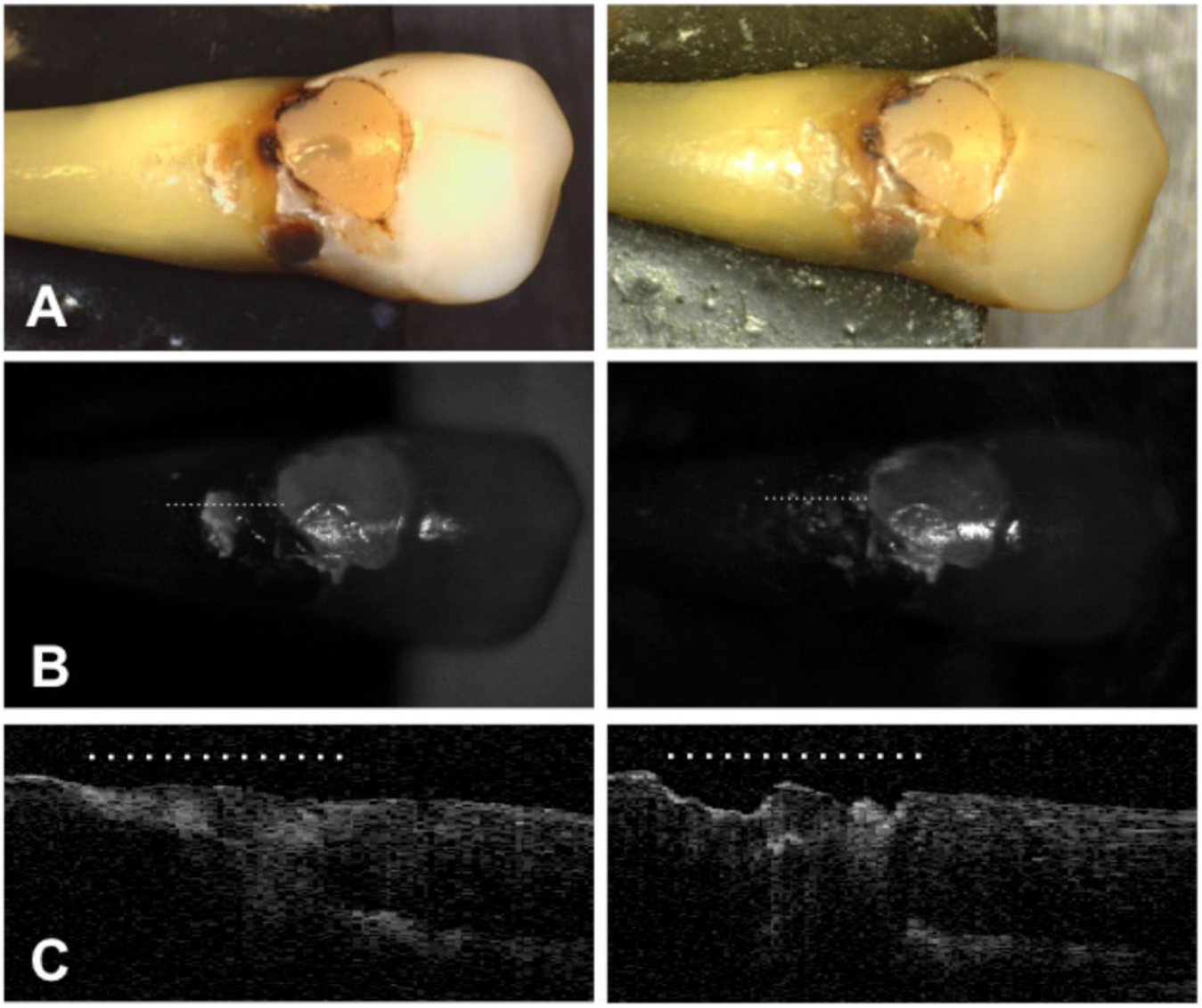

Fig. 4.

(A) Color and (B) SWIR (1 500–1750-nm) images and (C) OCT b-scans taken at the position of the dotted line in (B) before (left) and after (right) removal of demineralization. The dotted line in (B & C) shows the position of the OCT b-scan and the position of the lesion.